Journal of Sound and Vibration (2000) **232**(4), 783–806
doi:10.1006/jsvi.1999.2764, available online at http://www.idealibrary.com on IDEAL®

ONE-TO-ONE AUTO-PARAMETRIC RESONANCE IN SERPENTINE BELT DRIVE SYSTEMS

L. ZHANG AND J. W. ZU

Department of Mechanical and Industrial Engineering, University of Toronto, 5 King's College Road, Toronto, ON, Canada M5S 3G8

(*Received* 21 *January* 1999, *and in final form* 5 *November* 1999)

The coupled non-linear equations of motion of serpentine belt drive systems are solved using the direct multiple scales method. The entire hybrid system, which includes continuous belt spans, discrete pulleys, and tensioner arm, is divided into two subsystems. A one-to-one internal resonance combined with a primary external resonance is investigated. Solutions for the amplitude of non-trivial limit cycles are obtained. A stability analysis is performed on the steady state solutions. The quadratic non-linearity terms in the equations of motion are found to affect the belt drive systems significantly. It is shown that the direct multiple scales method yields better results for the system than the ordinary discretization multiple scales method. The effects of excitation frequencies, excitation amplitudes and the internal detuning parameter on dynamic responses are investigated.

1. INTRODUCTION

Serpentine belt drive systems have greatly improved reliability and maintenance requirement compared to multiple V-belt drives. However, such systems exhibit complex dynamic behavior, including rotational vibrations of pulleys with the belt spans serving as coupling springs, and transverse vibrations in the various belt spans. Therefore, it is of great interest to find an effective approach for modelling and predicting the dynamic response of serpentine belt drive systems.

Several recent studies have focused on the rotational vibration of serpentine belt drive systems. Hawker [1] investigated the natural frequencies of damped drive systems with a dynamic tensioner. Hwang *et al.* [2] proposed a general model for the rotational response of the entire serpentine belt drive system and applied the results to predict the onset of belt slip. For linear viscous damping, Kraver *et al.* [3] developed a complex procedure to solve both underdamped and overdamped systems. The above studies, however, all neglect transverse belt vibrations.

The transverse vibrations of belt spans can be modelled as an example of an axially moving material which has been investigated extensively [4–6]. Wickert and Mote [7] modified the classical modal analysis method by casting the equations of motion for a travelling string into a canonical, first order form. Moon and Wickert [8] developed a modal perturbation solution in the context of the asymptotic method of Krylov *et al.* for a continuous, non-autonomous and gyroscopic system with geometric non-linearity. More recently, Zhang and Zu [9, 10] studied the free and forced vibration of viscoelastic moving belts using the direct multiple scales method.

0022-460X/00/190783 + 24 $35.00/0

In the aforementioned studies, the coupling between the rotational and transverse vibration is not considered. However, Beikmann *et al.* [11] showed that there exists a linear mechanism coupling rotational vibration and transverse vibration of the belt spans adjacent to the tensioner arm. Zhang and Zu [12] derived the closed-form solution of eigenfunctions of a prototypical serpentine belt drive system. Beikmann *et al.* [13] demonstrated that non-linear coupling of rotational and transverse vibration arises from finite stretching of the belt. While such coupling is often small, it can become greatly magnified under conditions leading to an internal resonance. Since both quadratic and cubic non-linearities arise due to the non-linear coupling, and serpentine belt systems are hybrid systems with continuous and discrete components, it is challening to perform the non-linear analysis. In Beikmann's study [13], the two-to-one internal resonance is investigated using a numerical method. The non-linear vibration model was discretized using the linear eigenfunctions and the coupled vibration response was calculated using a Runge–Kutta method.

In this study, approximate analytical solutions are presented for the non-linear analysis of serpentine belt drive systems using the direct multiple scales method. Instead of assuming *a prior* linear spatial solution to describe the spatial solutions of the non-linear problems, the method of multiple scales is used to treat the continuous governing partial differential equations directly. Pakdemirli *et al.* [14] showed that direct perturbation methods yield better results for finite mode truncations and for systems having quadratic and cubic non-linearities. This is also demonstrated in the present study. The one-to-one internal resonance combined with a primary external resonance condition is investigated. The amplitude and phase modulation equations are obtained and the steady state response is derived. The quadratic non-linearity terms in the equations of motion are shown to influence the dynamic behavior of the system significantly. The effect of design parameters on the non-linear response is discussed.

2. EQUATIONS OF MOTION

A prototypical serpentine belt drive system developed by Beikmann *et al.* [11] is shown in Figure 1. The complete derivation of equations of motion governing this model is given by Biekmann [11]. The non-linearities considered here are geometric which describe finite stretching of the belt spans. The non-linear equations of motion are rewritten with the linear terms on the left side:

$$m(w_{i,tt} + 2cw_{i,xt}) - P_{ti}w_{i,xx} = P_{di}w_{i,xx}, \quad i = 1, 2, 3, \tag{1}$$

$$m_1\chi_{1,tt} + (k_1 + k_3)\chi_1 - k_1\chi_2 - k_1\cos\psi_1\chi_3 - k_3\chi_4 = P_{d1NL} - P_{d3NL} + F_{d1}, \tag{2}$$

$$m_2\chi_{2,tt} - k_1\chi_1 + (k_1 + k_2)\chi_2 + (k_1\cos\psi_1 - k_2\cos\psi_2)\chi_3 - k_2\chi_4 = P_{d2NL} - P_{d1NL}, \tag{3}$$

$$\begin{aligned} m_3\chi_{3,tt} &+ (P_{t1}w_{1,x}(l_1) - mcw_{1,t}(l_1))\sin\psi_1 + (-P_{t2}w_{2,x}(l_2) + mcw_{2,t}(l_2))\sin\psi_2 \\ &- k_1\cos\psi_1\chi_1 + (k_1\cos\psi_1 - k_2\cos\psi_2)\chi_2 + (k_1\cos^2\psi_1 + k_2\cos^2\psi_2 + k_4)\chi_3 \\ &+ k_2\cos\psi_2\chi_4 = -P_{d1NL}\cos\psi_1 - P_{d2NL}\cos\psi_2, \end{aligned} \tag{4}$$

$$m_4\chi_{4,tt} - k_3\chi_1 - k_2\chi_2 + k_2\cos\psi_2\chi_3 + (k_2 + k_3)\chi_4 = P_{d3NL} - P_{d2NL} + F_{d4}, \tag{5}$$

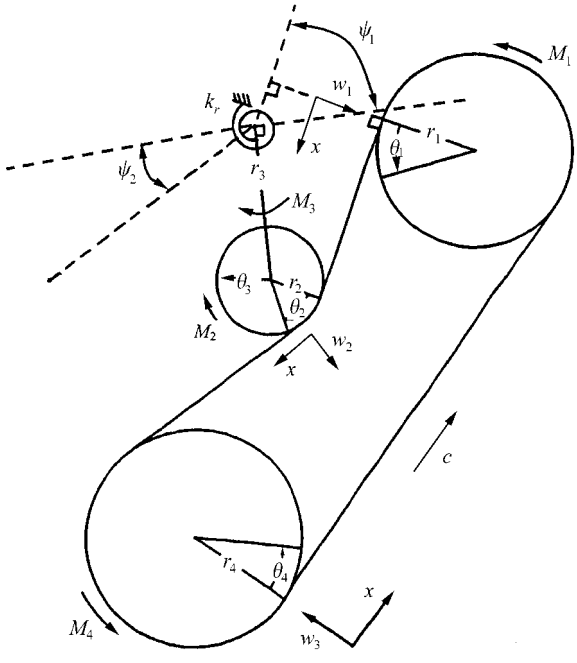

Figure 1. A prototypical three-pulley serpentine belt drive system.

where w_i is the transverse deflection in span i from equilibrium, m_i is the belt mass per unit length, P_{ti} is the span tractive tension component in span i at equilibrium ($P_{ti} - P_{oi} - mc^2$, where P_{oi} is the total operating tension in span i), l_i is the length of span i, $\chi_3(t)$ is the displacement of the tensioner pulley center along its arc, ψ_1 and ψ_2 are the alignment angles between the tensioner arm motion and the adjacent belt spans at equilibrium, $k_i = EA/l_i$ is the translational tensioner arm stiffness due to belt elongation, $F_{di} = M_{di}/r_i$ results from the applied dynamic moment on pulley i, and subscripts $_{,x}$ and $_{,t}$ denote the partial derivative with respect to x and t, respectively. The right-hand side of equations (1)–(5) include all non-linear and non-homogeneous (excitation) terms. P_{di} is the total dynamic tension in each span which can be separated into the linear component P_{diL} and the non-linear component P_{diNL}:

$$P_{di} = P_{diL} + P_{diNL}, \tag{6}$$

where

$$P_{diL} = k_i[u_i(l_i, t) - u_i(0, t)] \tag{7}$$

$$P_{diNL} = \frac{EA}{2l_i} \int_0^{l_i} w_{i,x}^2 \, \mathrm{d}x. \tag{8}$$

The non-linear equation (1) for the belt spans couples to equations (2)–(5) governing the four discrete elements (three pulleys and the tensioner arm). As shown in reference [12], for linear analysis, the transverse vibration of span 3 and the vibration of other components are decoupled. Thus, it is desirable to divide the entire system into two subsystems: subsystem 1 which includes span 3 only and subsystem 2 which includes all the other parts of the system.

For subsystem 1, the equation of motion is compactly written in the operator form as

$$M_3\ddot{w}_3 + G_3\dot{w}_3 + K_3 w_3 = F_3 \tag{9}$$

with boundary conditions

$$w_3(0, t) = 0, \qquad w_3(l_3, t) = 0, \tag{10}$$

where

$$M_3 = m, \qquad G_3 = 2mc\frac{\partial}{\partial x}, \qquad K_3 = -P_{t3}\frac{\partial^2}{\partial x^2}, \qquad F_3 = k_3(\chi_1 - \chi_4)w_{3,xx}. \tag{11}$$

For subsystem 2, the equations of motion can be rewritten in operator from

$$\mathbf{M}\ddot{\mathbf{W}} + \mathbf{G}\dot{\mathbf{W}} + \mathbf{K}\mathbf{W} = \mathbf{F}, \tag{12}$$

with boundaries

$$w_1(0, t) = 0, \qquad w_1(l_1, t) = \chi_3(t)\sin\psi_1, \tag{13}$$

$$w_2(0, t) = \chi_3(t)\sin\psi_2, \qquad w_2(l_2, t) = 0, \tag{14}$$

where $\mathbf{W}$ is composed of the transverse displacements $w_1(x, t)$ and $w_2(x, t)$ of the belt spans and the displacements $\chi_1(t)$, $\chi_2(t)$, $\chi_3(t)$ and $\chi_4(t)$ of the pulleys and tensioner arm; $\mathbf{M}$, $\mathbf{G}$ and $\mathbf{K}$ are linear matrix operators defined as

$$\mathbf{M} = \begin{bmatrix} m & 0 & 0 & 0 & 0 & 0 \\ 0 & m & 0 & 0 & 0 & 0 \\ 0 & 0 & m_1 & 0 & 0 & 0 \\ 0 & 0 & 0 & m_2 & 0 & 0 \\ 0 & 0 & 0 & 0 & m_3 & 0 \\ 0 & 0 & 0 & 0 & 0 & m_4 \end{bmatrix}, \tag{15}$$

$$\mathbf{G} = \begin{bmatrix} 2mc\dfrac{\partial}{\partial x} & 0 & 0 & 0 & 0 & 0 \\ 0 & 2mc\dfrac{\partial}{\partial x} & 0 & 0 & 0 & 0 \\ 0 & 0 & 0 & 0 & 0 & 0 \\ 0 & 0 & 0 & 0 & 0 & 0 \\ -mc\sin\psi_1|_{l_1} & mc\sin\psi_2|_0 & 0 & 0 & 0 & 0 \\ 0 & 0 & 0 & 0 & 0 & 0 \end{bmatrix}, \tag{16}$$

$$\mathbf{K} = \begin{bmatrix} -P_{t1}\dfrac{\partial^2}{\partial x^2} & 0 & 0 & 0 & 0 & 0 \\ 0 & -P_{t2}\dfrac{\partial^2}{\partial x^2} & 0 & 0 & 0 & 0 \\ 0 & 0 & k_1 + k_3 & -k_1 & -k_1\cos\psi_1 & -k_3 \\ 0 & 0 & -k_1 & k_1 + k_2 & k_1\cos\psi_1 - k_2\cos\psi_2 & -k_2 \\ P_{t1}\sin\psi_1\dfrac{\partial}{\partial x}\Big|_{l_1} & -P_{t2}\sin\psi_2\dfrac{\partial}{\partial x}\Big|_0 & -k_1\cos\psi_1 & k_1\cos\psi_1 - k_2\cos\psi_2 & k_1\cos^2\psi_1 + k_2\cos^2\psi_2 + k_4 & k_2\cos\psi_2 \\ 0 & 0 & -k_3 & -k_2 & k_2\cos\psi_2 & k_2 + k_3 \end{bmatrix} \tag{17}$$

and the vector $\mathbf{F}$ includes all non-homogeneous and non-linear terms:

$$\mathbf{F} = \begin{Bmatrix} P_{d1}w_{1,xx} \\ P_{d2}w_{2,xx} \\ P_{d1NL} - P_{d3NL} + F_{d1} \\ P_{d2NL} - P_{d1NL} \\ -P_{d2NL}\cos\psi_2 - P_{d1NL}\cos\psi_1 \\ P_{d3NL} - P_{d2NL} + F_{d4} \end{Bmatrix}. \tag{18}$$

The presence of boundary terms in $\mathbf{G}$ and $\mathbf{K}$ appears to break skew or symmetry. However, under the inner product definition $\langle \mathbf{W}_n, \mathbf{W}_r \rangle = \int_0^{t_1} w_{1n}\bar{w}_{1r}\,\mathrm{d}x + \int_0^{t_2} w_{2n}\bar{w}_{2r}\,\mathrm{d}x + \chi_n^{\mathrm{T}}\bar{\chi}_r$, the inner products $\langle \mathbf{W}, \mathbf{KW} \rangle$ and $\langle \mathbf{W}, \mathbf{GW} \rangle$ involve integrating terms by parts, which cancel with the non-zero boundary terms in $\mathbf{G}$ and $\mathbf{K}$. Therefore, the serpentine belt drive system operating at non-zero axial belt speed constitutes a conservative gyroscopic system.

Linear analysis shows that if two subsystems are given some initial conditions and allowed to oscillate freely, their response will be independent and each will vibrate with a constant amplitude. However, the two subsystems will interact strongly and exchange energy if an internal resonance condition is met. In addition, for subsystem 2, there may exist internal resonances between different modes. The following study will focus on the one-to-one internal resonance between the two subsystems combined with a primary external resonance while the internal resonance within subsystem 2 will not be considered.

3. DIRECT MULTIPLE SCALES METHOD

The method of multiple scales is ideally stuited to the study of equations (9) and (12), which contain both quadratic and cubic non-linearities. A solution uniformly valid up to third order for equations (9) and (12) is presented by assuming an expansion of the form

$$w_3 = \varepsilon w_{31}(T_0, T_1, T_3) + \varepsilon^2 w_{32}(T_0, T_1, T_2) + \varepsilon^3 w_{33}(T_0, T_1, T_3) + \cdots, \tag{19}$$

$$\mathbf{W} = \varepsilon \mathbf{W}_1(T_0, T_1, T_2) + \varepsilon^2 \mathbf{W}_2(T_0, T_1, T_2) + \varepsilon^3 \mathbf{W}_3(T_0, T_1, T_2) + \cdots, \tag{20}$$

where w_{3i} and $\mathbf{W}_i$ are $O(1)$, ε is a small dimensionless measure of the amplitude of response used as a bookkeeping device, $T_0 = t$ is the fast-time scale whereas $T_1 = \varepsilon t$ and $T_2 = \varepsilon^2 t$ are

the slow-time scales. The external excitations are reordered so that their effects balance the effect of non-linearity, that is

$$F_{d1} = \varepsilon^3 \hat{F}_{d1}, \qquad F_{d4} = \varepsilon^3 \hat{F}_{d4}, \tag{21}$$

where $\hat{F}_{d1}$ and $\hat{F}_{d4}$ are equivalent to F_{d1} and F_{d4} since ε is a bookkeeping device.

The time derivatives can be written in terms of the T_n $(n = 0, 1, \ldots)$ as

$$\frac{\partial}{\partial t} = \frac{\partial}{\partial T_0} + \varepsilon \frac{\partial}{\partial T_1} + \varepsilon^2 \frac{\partial}{\partial T_2} + \cdots, \tag{22}$$

$$\frac{\partial^2}{\partial t^2} = \frac{\partial^2}{\partial T_0^2} + 2\varepsilon \frac{\partial^2}{\partial T_0 \partial T_1} + \varepsilon^2 \left(\frac{\partial^2}{\partial T_1^2} + 2 \frac{\partial^2}{\partial T_0 \partial T_2} \right) + \cdots. \tag{23}$$

Substituting equations (21)–(23) into equations (9)–(12) and equating coefficients of like powers of ε yields the following.

Order ε, *subsystem* 1:

$$M_3 \frac{\partial^2 w_{31}}{\partial T_0^2} + G_3 \frac{\partial w_{31}}{\partial T_0} + K_3 w_{31} = 0, \tag{24}$$

$$w_{31}(0, t) = 0, \qquad w_{31}(l_3, t) = 0. \tag{25}$$

Order ε, *subsystem* 2:

$$\mathbf{M} \frac{\partial^2 \mathbf{W}_1}{\partial T_0^2} + \mathbf{G} \frac{\partial \mathbf{W}_1}{\partial T_0^2} + \mathbf{K} \mathbf{W}_1 = \mathbf{0}, \tag{26}$$

$$w_{11}(0, t) = 0, \qquad w_{11}(l_1, t) = \chi_{31}(t) \sin \psi_1, \tag{27}$$

$$w_{21}(0, t) = \chi_{31}(t) \sin \psi_2, \qquad w_{21}(l_2, t) = 0. \tag{28}$$

Order ε^2, *subsystem* 1:

$$M_3 \frac{\partial^2 w_{32}}{\partial T_0^2} + G_3 \frac{\partial w_{32}}{\partial T_0} + K_3 w_{32} = -2M_3 \frac{\partial^2 w_{31}}{\partial T_0 \partial T_1} - G_3 \frac{\partial w_{31}}{\partial T_1} + N_{Q3}, \tag{29}$$

$$w_{32}(0, t) = 0, \qquad w_{32}(l_3, t) = 0, \tag{30}$$

where

$$N_{Q3} = k_3(\chi_{11} - \chi_{41}) w_{31,xx}. \tag{31}$$

Order ε^2, *subsystem* 2:

$$\mathbf{M} \frac{\partial^2 \mathbf{W}_2}{\partial T_0^2} + \mathbf{G} \frac{\partial W_2}{\partial T_0} + \mathbf{K} \mathbf{W}_2 = -\mathbf{2M} \frac{\partial^2 \mathbf{W}_1}{\partial T_0 \partial T_1} - \mathbf{G} \frac{\partial \mathbf{W}_1}{\partial T_1} + \mathbf{N}_Q, \tag{32}$$

$$w_{12}(0, t) = 0, \qquad w_{12}(l_1, t) = \chi_{32}(t) \sin \psi_1, \tag{33}$$

$$w_{22}(0, t) = \chi_{32}(t) \sin \psi_2, \qquad w_{22}(l_2, t) = 0, \tag{34}$$

where

$$\mathbf{N}_Q = \left\{ \begin{array}{c} k_1(\chi_{31}\cos\psi_1 + \chi_{21} - \chi_{11})w_{11,xx} \\ k_2(\chi_{31}\cos\psi_2 + \chi_{41} - \chi_{21})w_{21,xx} \\ \dfrac{EA}{2l_1}\displaystyle\int_0^{l_1} w_{11,x}^2\,\mathrm{d}x - \dfrac{EA}{2l_3}\int_0^{l_3} w_{31,x}^2\,\mathrm{d}x \\ \dfrac{EA}{2l_2}\displaystyle\int_0^{l_2} w_{21,x}^2\,\mathrm{d}x - \dfrac{EA}{2l_1}\int_0^{l_1} w_{11,x}^2\,\mathrm{d}x \\ -\dfrac{EA}{2l_2}\displaystyle\int_0^{l_2} w_{21,x}^2\,\mathrm{d}x\cos\psi_2 - \dfrac{EA}{2l_2}\int_0^{l_1} w_{11,x}^2\,\mathrm{d}x\cos\psi_1 \\ \dfrac{EA}{2l_3}\displaystyle\int_0^{l_3} w_{31,x}^2\,\mathrm{d}x - \dfrac{EA}{2l_2}\int_0^{l_2} w_{21,x}^2\,\mathrm{d}x \end{array} \right\}. \tag{35}$$

Order ε^3, *subsystem* 1:

$$M_3\frac{\partial^2 w_{33}}{\partial T_0^2} + G_3\frac{\partial w_{33}}{\partial T_0} + K_3 w_{33} = -M_3\left(2\frac{\partial^2 w_{31}}{\partial T_0\partial T_2} + \frac{\partial^2 w_{31}}{\partial T_1^2} + 2\frac{\partial^2 w_{32}}{\partial T_0\partial T_1}\right)$$

$$- G_3\left(\frac{\partial w_{31}}{\partial T_2} + \frac{\partial w_{32}}{\partial T_1}\right) + N_{C3}, \tag{36}$$

$$w_{33}(0,t) = 0, \qquad w_{33}(l_3,t) = 0, \tag{37}$$

where

$$N_{C3} = k_3(\chi_{11} - \chi_{41})w_{32,xx} + k_3(\chi_{12} - \chi_{42})w_{31,xx} + \frac{EA}{2l_3}\int_0^{l_3} w_{31,x}^2\,\mathrm{d}x\,w_{31,xx}. \tag{38}$$

Order ε^3, *subsystem* 2:

$$\mathbf{M}\frac{\partial^2 \mathbf{W}_3}{\partial T_0^2} + \mathbf{G}\frac{\partial \mathbf{W}_3}{\partial T_0} + \mathbf{K}\mathbf{W}_3 = -\mathbf{M}\left(2\frac{\partial^2 \mathbf{W}_1}{\partial T_0\partial T_2} + \frac{\partial^2 \mathbf{W}_1}{\partial T_1^2} + 2\frac{\partial^2 \mathbf{W}_2}{\partial T_0\partial T_1}\right)$$

$$- \mathbf{G}\left(\frac{\partial \mathbf{W}_1}{\partial T_2} + \frac{\partial \mathbf{W}_2}{\partial T_1}\right) + \mathbf{N}_C, \tag{39}$$

$$w_{13}(0,t) = 0, \qquad w_{13}(l_1,t) = \chi_{33}(t)\sin\psi_1, \tag{40}$$

$$w_{23}(0,t) = \chi_{33}(t)\sin\psi_2, \qquad w_{23}(l_2,t) = 0, \tag{41}$$

where

$$\mathbf{N}_C = \left\{ \begin{array}{c} k_1(\chi_{31}\cos\psi_1+\chi_{21}-\chi_{11})w_{12,xx}+k_1(\chi_{32}\cos\psi_1+\chi_{22}-\chi_{12})w_{11,xx}+\dfrac{EA}{2l_1}\displaystyle\int_0^{l_1} w_{11,x}^2\,\mathrm{d}x\,w_{11,xx} \\ k_2(\chi_{31}\cos\psi_2+\chi_{41}-\chi_{21})w_{22,xx}+k_2(\chi_{32}\cos\psi_2+\chi_{42}-\chi_{22})w_{21,xx}+\dfrac{EA}{2l_2}\displaystyle\int_0^{l_2} w_{21,x}^2\,\mathrm{d}x\,w_{21,xx} \\ \dfrac{EA}{l_1}\displaystyle\int_0^{l_1} w_{11,x}w_{12,x}\,\mathrm{d}x-\dfrac{EA}{l_3}\displaystyle\int_0^{l_3} w_{31,x}w_{32,x}\,\mathrm{d}x+\hat{F}_{d1} \\ \dfrac{EA}{l_2}\displaystyle\int_0^{l_2} w_{21,x}w_{22,x}\,\mathrm{d}x-\dfrac{EA}{l_1}\displaystyle\int_0^{l_1} w_{11,x}w_{12,x}\,\mathrm{d}x \\ -\dfrac{EA}{l_2}\displaystyle\int_0^{l_2} w_{21,x}w_{22,x}\,\mathrm{d}x\cos\psi_2-\dfrac{EA}{l_1}\displaystyle\int_0^{l_1} w_{11,x}w_{12,x}\,\mathrm{d}x\cos\psi_1 \\ \dfrac{EA}{l_3}\displaystyle\int_0^{l_3} w_{31,x}w_{32,x}\,\mathrm{d}x-\dfrac{EA}{l_2}\displaystyle\int_0^{l_2} w_{21,x}w_{22,x}\,\mathrm{d}x+\hat{F}_{d4} \end{array} \right\}. \tag{42}$$

Consider the case in which subsystem 2 is excited by a primary external resonance and subsystem 1 is excited indirectly by internal resonance. Hence, the solutions of equations (24) and (26) are sought in the form

$$w_{31} = \varphi_m B_m(T_1, T_2)\mathrm{e}^{\mathrm{i}\lambda_m T_0} + cc, \qquad \mathbf{W}_1 = \boldsymbol{\phi}_n \mathbf{A}_n(\mathbf{T}_1, \mathbf{T}_2)\mathrm{e}^{\mathrm{i}\omega_n T_0} + cc, \tag{43, 44}$$

where cc stands for the complex conjugate of the preceding terms, λ_m and ω_n are the eigenvalues associated with subsystems 1 and 2, respectively, $\boldsymbol{\phi}_n(x)$ and $\varphi_m(x)$ are the corresponding eigenfunctions, and A_n and B_n are complex functions yet to be determined.

4. ONE-TO-ONE INTERNAL RESONANCE

In serpentine belt drive systems, due to the quadratic and cubic non-linearities, both two-to-one and one-to-one resonances are possible. Generally, a two-to-one resonance poses a more serious threat to the drive system than a one-to-one resonance. However, in some cases, the one-to-one resonance can also cause large belt deflection. In Beikmann's experiment [15], linear coupling between the pulley rotation and the transverse motion of span 3 is found. It seems that this linear coupling may influence the one-to-one resonance characteristics. In this study, however, only the one-to-one internal resonance due to the non-linearity is considered. To quantitatively describe a primary external resonance and a one-to-one internal resonance, two detuning parameters σ_1 and σ_2 are introduced, defined by

$$\omega_n = \lambda_m + \varepsilon^2\sigma_1, \qquad \Omega = \omega_n + \varepsilon^2\sigma_2, \tag{45}$$

where Ω is the frequency of external excitation.

Substituting equations (43) and (44) into equations (31) and (35), it is noted that for one-to-one internal resonance there are no secular terms arising from $\mathbf{N}_Q$ and N_{Q3}.

Therefore, the solvability conditions for equations (29) and (32) are

$$\langle -(2\mathrm{i}\lambda_m M_3 \varphi_m + G_3 \varphi_m), \varphi_m \rangle \frac{\partial B_m}{\partial T_1} = 0, \tag{46}$$

$$\langle -(2\mathrm{i}\omega_n \mathbf{M}\boldsymbol{\phi}_n + \mathbf{G}\boldsymbol{\phi}_n), \boldsymbol{\phi}_n \rangle \frac{\partial A_n}{\partial T_1} = 0. \tag{47}$$

Inserting the expression of $\boldsymbol{\phi}_n$ and φ_m into equations (46) and (47) results in

$$\frac{\partial A_n}{\partial T_1} = 0, \qquad \frac{\partial B_m}{\partial T_1} = 0. \tag{48}$$

Therefore, $A_n = A_n(T_2)$ and $B_m = B_m(T_2)$ only. This shows that for one-to-one internal resonance, there is no $T_1 = \varepsilon t$ dependence.

After eliminating the secular terms, the solutions of equations (29) and (32) can be assumed to be of the form

$$w_{32} = \gamma_{51}(x) A_n B_m \mathrm{e}^{\mathrm{i}(\omega_n + \lambda_m)T_0} + \gamma_{61}(x) A_n B_m \mathrm{e}^{\mathrm{i}(\omega_n - \lambda_m)T_0} + cc, \tag{49}$$

$$\mathbf{W}_2 = \left(\begin{Bmatrix} \gamma_{11}(x) \\ \gamma_{12}(x) \\ \gamma_{13} \\ \gamma_{14} \\ \gamma_{15} \\ \gamma_{16} \end{Bmatrix} A_n^2 \mathrm{e}^{\mathrm{i}\omega_n T_0} + cc \right) + \begin{Bmatrix} \gamma_{21}(x) \\ \gamma_{22}(x) \\ \gamma_{23} \\ \gamma_{24} \\ \gamma_{25} \\ \gamma_{26} \end{Bmatrix} A_n \bar{A}_n + \left(\begin{Bmatrix} \gamma_{31}(x) \\ \gamma_{32}(x) \\ \gamma_{33} \\ \gamma_{34} \\ \gamma_{35} \\ \gamma_{36} \end{Bmatrix} B_m^2 \mathrm{e}^{2\mathrm{i}\lambda_m T_0} + cc \right)$$

$$+ \begin{Bmatrix} \gamma_{41}(x) \\ \gamma_{42}(x) \\ \gamma_{43} \\ \gamma_{44} \\ \gamma_{45} \\ \gamma_{46} \end{Bmatrix} B_m \bar{B}_m, \tag{50}$$

where the γ_{ij} capture the spatial dependence of the motion. Substituting equations (49) and (50) into equations (29) and (32), γ_{ij} can be obtained by solving the ordinary differential boundary value problems.

It is apparent that the spatial variation of the second order terms is different from those of the linear solutions. Hence, the validity of the assumption that the spatial variation of higher order solutions is the same as that of the first order solutions is highly questionable. However, this assumption is made prior to the discretization multiple scales method.

Substituting equations (43), (44), (49) and (50) into equations (38) and (42) leads to

$$N_{C3} = (\Gamma_{41} A_n^2 \bar{B}_m \mathrm{e}^{2\mathrm{i}\sigma_1 T_2} + \Gamma_{51} A_n \bar{A}_n B_m + \Gamma_{61} B_m^2 \bar{B}_m)\mathrm{e}^{\mathrm{i}\lambda_m T_0} + NST3, \tag{51}$$

$$\mathbf{N}_C = \left(\begin{Bmatrix} \Gamma_{11} \\ \Gamma_{12} \\ \Gamma_{13} \\ \Gamma_{14} \\ \Gamma_{15} \\ \Gamma_{16} \end{Bmatrix} A_n^2 \bar{A}_n + \begin{Bmatrix} \Gamma_{21} \\ \Gamma_{22} \\ \Gamma_{23} \\ \Gamma_{24} \\ \Gamma_{25} \\ \Gamma_{26} \end{Bmatrix} A_n B_m \bar{B}_m + \begin{Bmatrix} \Gamma_{31} \\ \Gamma_{32} \\ \Gamma_{33} \\ \Gamma_{34} \\ \Gamma_{35} \\ \Gamma_{36} \end{Bmatrix} \bar{A}_n B_m^2 \mathrm{e}^{-2\mathrm{i}\sigma_1 T_2} + \begin{Bmatrix} 0 \\ 0 \\ \hat{F}_{d1} \\ 0 \\ 0 \\ \hat{F}_{d4} \end{Bmatrix} \mathrm{e}^{\mathrm{i}\sigma_2 T_2} \right) \mathrm{e}^{\mathrm{i}\omega_n T_0} + \mathbf{NST}, \tag{52}$$

where $NST3$ and **NST** denote non-secular terms and Γ_{ij} is given in Appendix A.

Because the homogeneous part of equations (36)–(41) has a non-trivial solution, the inhomogeneous equations have a solution only if a solvability condition is satisfied. The solvability conditions for equations (36)–(41) are found to be as follows:

$$-M_G \frac{\partial A_n}{\partial T_2} + A_n^2 \bar{A}_n \Theta_1 + A_n B_m \bar{B}_m \Theta_2 + \bar{A}_n B_m^2 \mathrm{e}^{-2\mathrm{i}\sigma_1 T_2} \Theta_3 + (\hat{F}_{d1} \hat{\chi}_{1n} + \hat{F}_{d4} \hat{\chi}_{4n})\mathrm{e}^{\mathrm{i}\sigma_2 T_2} - 2\mathrm{i}\hat{\zeta}_n A_n = 0, \tag{53}$$

$$-M_{3G} \frac{\partial B_m}{\partial T_2} + A_n^2 \bar{B}_m \mathrm{e}^{2\mathrm{i}\sigma_1 T_2} \Theta_4 + A_n \bar{A}_n B_m \Theta_5 + B_m^2 \bar{B}_m \Theta_6 - 2\mathrm{i}\hat{\zeta}_m B_m = 0, \tag{54}$$

where $\hat{\zeta}_n$ and $\hat{\zeta}_m$ are modal damping and

$$M_G = \frac{2\mathrm{i}}{\omega_n}, \qquad M_{3G} = \frac{2\mathrm{i}}{\lambda_m}, \tag{55}$$

$$\Theta_1 = \int_0^{l_1} \Gamma_{11} \bar{\phi}_{1n} \mathrm{d}x + \int_0^{l_2} \Gamma_{12} \bar{\phi}_{2n} \mathrm{d}x + \Gamma_{13} \hat{\chi}_{1n} + \Gamma_{14} \hat{\chi}_{2n} + \Gamma_{15} \hat{\chi}_{3n} + \Gamma_{16} \hat{\chi}_{4n}, \tag{56}$$

$$\Theta_2 = \int_0^{l_1} \Gamma_{21} \bar{\phi}_{1n} \mathrm{d}x + \int_0^{l_2} \Gamma_{22} \bar{\phi}_{2n} \mathrm{d}x + \Gamma_{23} \hat{\chi}_{1n} + \Gamma_{24} \hat{\chi}_{2n} + \Gamma_{25} \hat{\chi}_{3n} + \Gamma_{26} \hat{\chi}_{4n}, \tag{57}$$

$$\Theta_3 = \int_0^{l_1} \Gamma_{31} \bar{\phi}_{1n} \mathrm{d}x + \int_0^{l_2} \Gamma_{32} \bar{\phi}_{2n} \mathrm{d}x + \Gamma_{33} \hat{\chi}_{1n} + \Gamma_{34} \hat{\chi}_{2n} + \Gamma_{35} \hat{\chi}_{3n} + \Gamma_{36} \hat{\chi}_{4n}, \tag{58}$$

$$\Theta_4 = \int_0^{l_3} \Gamma_{41} \bar{\varphi}_m \mathrm{d}x, \qquad \Theta_5 = \int_0^{l_3} \Gamma_{51} \bar{\varphi}_m \mathrm{d}x, \qquad \Theta_6 = \int_0^{l_3} \Gamma_{61} \bar{\varphi}_m \mathrm{d}x. \tag{59–61}$$

Equations (53) and (54) govern the time evolution of the amplitudes and phases of the response. The terms Θ_i defined in equations (55)–(61) are composed of integrals of the spatial solutions determined at the first and second orders. Thus, the spatial solutions have strong influence on the evolution of the complex amplitudes A_n and B_m. Since the spatial

variation of the second order is different from that of the first order, there exist discrepancies between the direct approach and the discretization approach.

We may express the complex amplitudes A_n and B_m in the polar form

$$A_n = \tfrac{1}{2}\alpha_n e^{i\beta_n}, \qquad B_m = \tfrac{1}{2}\alpha_m e^{i\beta_m}. \tag{62}$$

Substituting this polar form into equations (53) and (54), the separating the result into real and imaginary parts, the first order differential equations for the amplitudes and phases are obtained as

$$\frac{\partial \alpha_n}{\partial T_2} - \omega_n \frac{\mathrm{Im}(\Theta_1)}{8}\alpha_m^3 - \omega_n \frac{\mathrm{Im}(\Theta_2)}{8}\alpha_n \alpha_m^2 - \omega_n \frac{\mathrm{Im}(\Theta_3)\cos\zeta_1 - \mathrm{Re}(\Theta_3)\sin\zeta_1}{8}\alpha_n \alpha_m^2 - F_d \sin\zeta_2 + \omega_n \zeta_n \alpha_n = 0, \tag{63}$$

$$\alpha_n\left(\sigma_2 - \frac{\partial \zeta_2}{\partial T_2}\right) + \omega_n \frac{\mathrm{Re}(\Theta_1)}{8}\alpha_n^3 + \omega_n \frac{\mathrm{Re}(\Theta_2)}{8}\alpha_n \alpha_m^2 + \omega_n \frac{\mathrm{Re}(\Theta_3)\cos\zeta_1 + \mathrm{Im}(\Theta_3)\sin\zeta_1}{8}\alpha_n \alpha_m^2 + F_d \cos\zeta_2 = 0, \tag{64}$$

$$\frac{\partial \alpha_m}{\partial T_2} - \lambda_m \frac{\mathrm{Im}(\Theta_6)}{8}\alpha_m^3 - \lambda_m \frac{\mathrm{Im}(\Theta_5)}{8}\alpha_n^2 \alpha_m - \lambda_m \frac{\mathrm{Im}(\Theta_4)\cos\zeta_1 + \mathrm{Re}(\Theta_4)\sin\zeta_1}{8}\alpha_n^2 \alpha_m + \lambda_m \hat{\zeta}_m \alpha_m = 0, \tag{65}$$

$$\alpha_m\left(\sigma_1 + \sigma_2 - \frac{1}{2}\frac{\partial \zeta_1}{\partial T_2} - \frac{\partial \zeta_2}{\partial T_2}\right) + \lambda_m \frac{\mathrm{Re}(\Theta_6)}{8}\alpha_m^3 + \lambda_m \frac{\mathrm{Re}(\Theta_5)}{8}\alpha_n^2 \alpha_m + \lambda_m \frac{\mathrm{Re}(\Theta_4)\cos\zeta_1 - \mathrm{Im}(\Theta_4)\sin\zeta_1}{8}\alpha_n^2 \alpha_m = 0, \tag{66}$$

where Re( ) and Im( ) denote the real and imaginary parts of a complex variable and

$$\zeta_1 = 2(\beta_n - \beta_m + \sigma_1 T_2), \qquad \zeta_2 = \sigma_2 T_2 - \beta_n, \tag{67}$$

$$F_d = \omega_n(\hat{\chi}_{1n}\hat{F}_{d1} + \hat{\chi}_{4n}\hat{F}_{d4}), \tag{68}$$

where $\hat{\chi}_{1n}$ and $\hat{\chi}_{4n}$ are the normalized modal components corresponding to pulley's 1 and 4, respectively.

For the steady state response, the amplitude α_n and α_m and the new phase angle ζ_1 and ζ_2 in equations (86)–(89) should be constant. Thus, setting $\partial\alpha_n/\partial T_2 = \partial\alpha_m/\partial T_2 = \partial\zeta_1/\partial T_2 = \partial\zeta_2/\partial T_2 = 0$ and with some manipulations, the amplitude and phase of the steady state response can be determined from the following algebraic equations:

$$-\omega_n \frac{\mathrm{Im}(\Theta_1)}{8}\alpha_n^3 - \omega_n \frac{\mathrm{Im}(\Theta_2)}{8}\alpha_n \alpha_m^2 - \omega_n \frac{\mathrm{Im}(\Theta_3)\cos\zeta_1 - \mathrm{Re}(\Theta_3)\sin\zeta_1}{8}\alpha_n \alpha_m^2 - F_d \sin\zeta_2 + \omega_n \zeta_n \alpha_n = 0, \tag{69}$$

$$\alpha_n\sigma_2 + \omega_n \frac{\mathrm{Re}(\Theta_1)}{8}\alpha_n^3 + \omega_n \frac{\mathrm{Re}(\Theta_2)}{8}\alpha_n\alpha_m^2 + \omega_n \frac{\mathrm{Re}(\Theta_3)\cos\zeta_1 + \mathrm{Im}(\Theta_3)\sin\zeta_1}{8}\alpha_n\alpha_m^2 + F_d\cos\zeta_2 = 0, \tag{70}$$

$$-\lambda_m \frac{\mathrm{Im}(\Theta_6)}{8}\alpha_m^3 - \lambda_m \frac{\mathrm{Im}(\Theta_5)}{8}\alpha_n^2\alpha_m - \lambda_m \frac{\mathrm{Im}(\Theta_4)\cos\zeta_1 + \mathrm{Re}(\Theta_4)\sin\zeta_1}{8}\alpha_n^2\alpha_m + \lambda_m\hat{\zeta}_m\alpha_m = 0, \tag{71}$$

$$\alpha_m(\sigma_1 + \sigma_2) + \lambda_m \frac{\mathrm{Re}(\Theta_6)}{8}\alpha_m^3 + \lambda_m \frac{\mathrm{Re}(\Theta_5)}{8}\alpha_n^2\alpha_m + \lambda_m \frac{\mathrm{Re}(\Theta_4)\cos\zeta_1 - \mathrm{Im}(\Theta_4)\sin\zeta_1}{8}\alpha_n^2\alpha_m = 0. \tag{72}$$

For the second order approximation, the response of subsystems 1 and 2 can be calculated by inserting equations (43), (44), (49) and (50) into equations (16) and (17).

TABLE 1

The physical properties for the prototypical systems

	Pulley 1	Pulley 2	Tensioner arm	Pulley 4
Spin axis coordinates	(0·5525, 0·0556)	(0·3477, 0·05715)	(0·2508, 0·0635)	(0·0, 0·0)
Radii (m)	0·0889	0·0452	0·097	0·02697
Rotational inertia (kg m^2)	0·07248	0·00293	0·001165	0·000293
Other physical properties	Belt modulus: $EA = 170\,000$ N, $m = 0{\cdot}1029$ kg/m Tensioner spring constant: $k_r = 54{\cdot}37$ N m/rad			

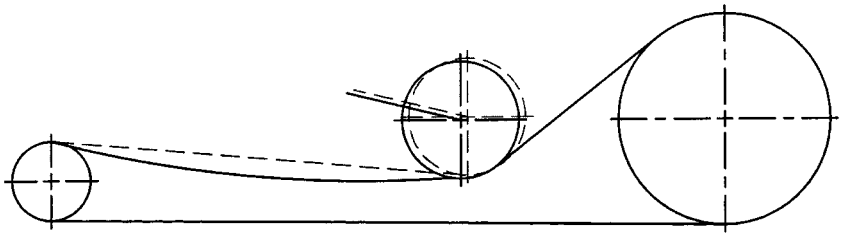

Figure 2. The rotational mode of subsystem 1: – – –, original system; —— mode shape.

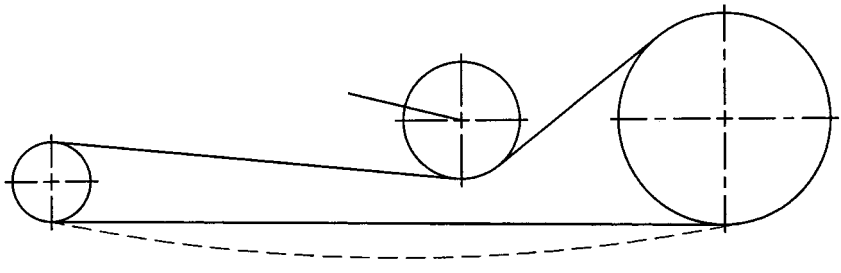

Figure 3. The transverse mode of subsystem 2: ——, original system; – – – mode shape.

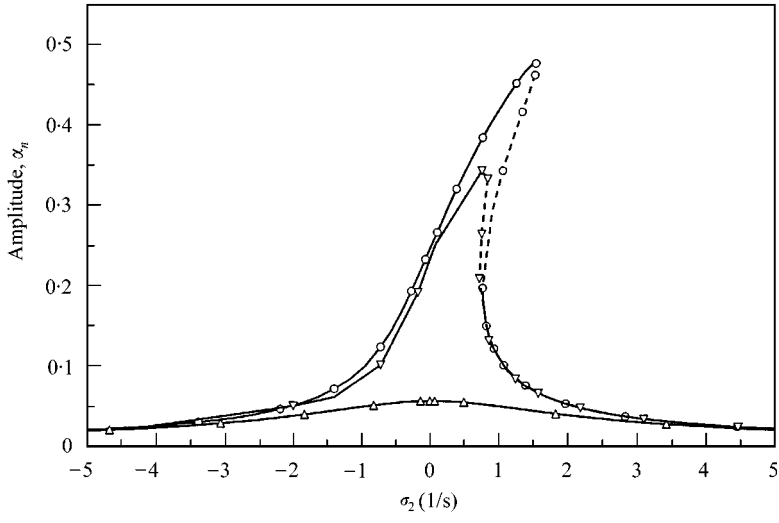

Figure 4. Frequency-response curves of the rotational mode obtained by the direct multiple scales method in the case of zero belt 3 motion: —○—, $\zeta_n = 0{\cdot}0$, stable; - -○- -, $\zeta_n = 0{\cdot}0$, unstable; —▽—, $\zeta_n = 0{\cdot}1\%$, stable; - -▽- -, $\zeta_n = 0{\cdot}1\%$, unstable; —△—, $\zeta_n = 1{\cdot}0\%$, stable.

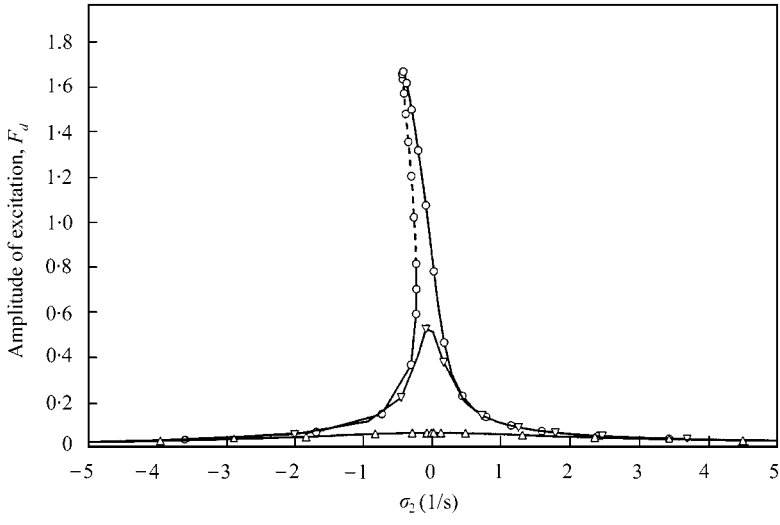

Figure 5. Frequency-response curves of the rotational mode obtained by the discretization multiple scales method in the case of zero belt 3 motion: —○—, $\zeta_n = 0{\cdot}0$, stable; - -○- -, $\zeta_n = 0{\cdot}0$, unstable; —▽—, $\zeta_n = 0{\cdot}1\%$ stable; —△—, $\zeta_n = 1{\cdot}0\%$, unstable.

5. NUMERICAL EXAMPLES

A comparison is made between the direct multiple scales method and discretization multiple scales method. The prototypical system used in this simulation is identical to that proposed by Beikmann [13]. The physical properties of the system are shown in Table 1. An addition of 2·15 kg mass is added to the tensioner arm, at the tensioner pulley axis. This

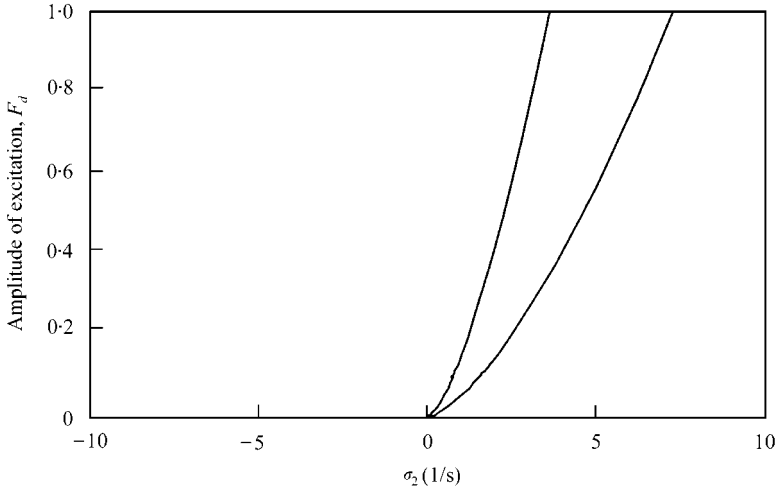

Figure 6. Multi-valued region obtained by direct multiple scales method when $\alpha_m = 0$, $\hat{\zeta}_n = 0$, $\hat{\zeta}_m = 0$.

mass only servers the purpose of reducing the natural frequency of the rotational mode. The operating speed is 2000 r.p.m. The frequency of the first transverse mode of span 3 is 28·1104 Hz and the frequency of the first rotationally dominant mode is 29·0590 Hz.

The rotational mode of subsystem 1 is shown in Figure 2, and the transverse mode of subsystem 2 (belt span 3) is shown in Figure 3. The solid line denotes the mode shape and the dashed line denotes the original system. The figures indicate that there is a significant coupling between the span's transverse mode and the pulley's rotational mode.

In the case of no transverse vibration of span 3, Figures 4 and 5 present the amplitude curves of α_n of the rotational mode versus σ_2 for different values of modal damping calculated by the direct multiple scales method and the discretization multiple scales method respectively. Figure 6 shows the region where there exists multi-valued amplitudes for zero damping. Within the region bounded by the two curves, there are three rest states and outside of the two curves there is only one steady state solution.

Comparison between Figure 4 and Figure 5 shows that the two approaches yield qualitatively different predictions of the system response. For the direct multiple scales method, the dominance of the cubic non-linearity leads to the hardening behavior shown in Figure 4. For discretization multiple scales method, the dominance of quadratic non-linearity is evident from the softening behavior shown in Figure 5. The steady state responses of direct multiple scales appear to be more reasonable since the one-to-one internal resonance results from the cubic non-linearity.

In the case of $\alpha^m \neq 0$, the solution curves for α_n and α_m by two approaches are shown in Figures 7 and 8. The modal damping for the rotational mode is 1% and for transverse mode is 0·3%. It is seen that three branch curves exist for α_n within a certain range of the detuning parameter σ_2. The highest branch corresponds to the case of no transverse vibration of span 3. The presence of the cubic non-linearity causes distortion and asymmetry in these curves. There always exist two steady state solutions for α_n within the range where non-trivial solutions exist. The difference between the two steady state solutions for α_n approaches zero as σ_2 becomes smaller. Two steady state solutions are possible for α_m within a certain range of σ_2 values.

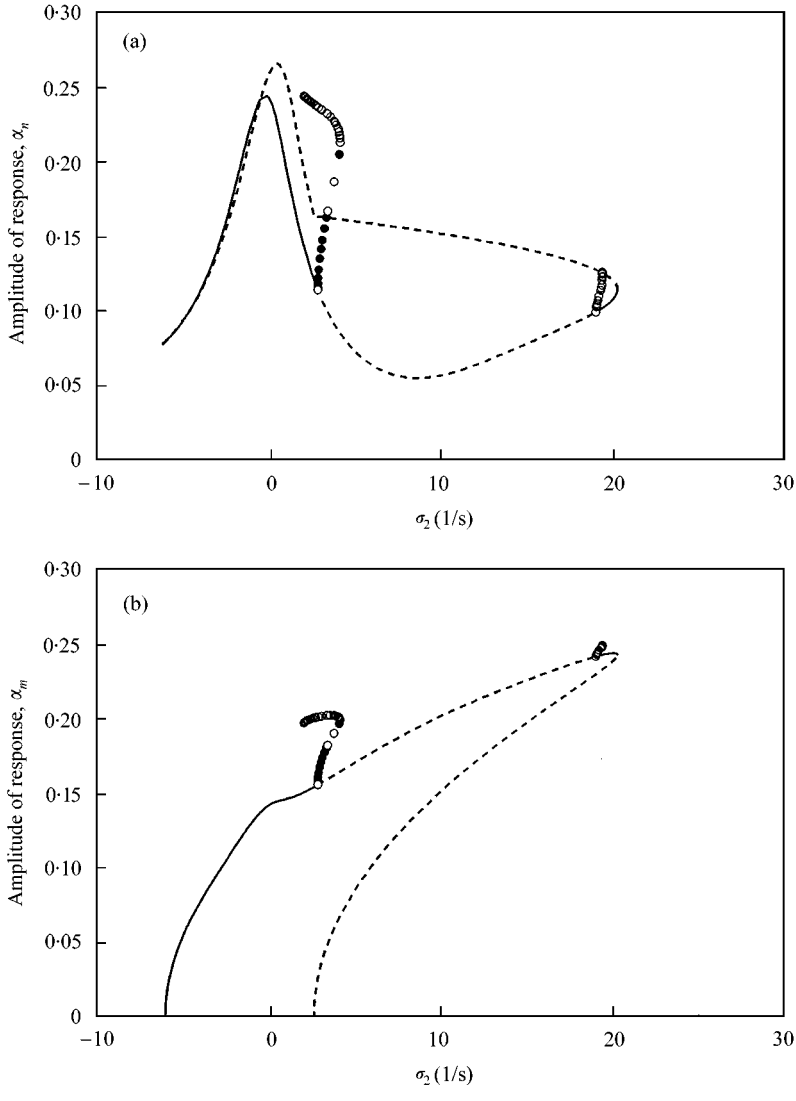

Figure 7. Frequency-response curves obtained by the direct multiple scales method, $\alpha_m \neq 0$, $\hat{\zeta}_n = 1\%$; $\hat{\zeta}_m = 0{\cdot}3\%$. (a) Amplitude of the rotational mode, (b) amplitude of the transverse mode of span 3: —, stable fixed points, - - - -, unstable fixed points; ●, stable periodic solutions; ○, unstable periodic solutions.

There are two sets of Hopf bifurcations emanating from the steady state solutions, which lead to oscillating amplitudes and phases. Filled circles represent stable periodic orbits and open circles are unstable.

It is evident that the responses for α_n and α_m obtained from the direct multiple scales method are quite different from those obtained from the discretization multiple scales method. For the discretization multiple scales method, two branch curves exist for α_n and α_m on both sides of $\sigma_2 = 0$, which is typical of a coupled system with quadratic non-linearity. For the direct multiple scales method, the distortion and asymmetry caused by the cubic non-linearity seems to be more dominant.

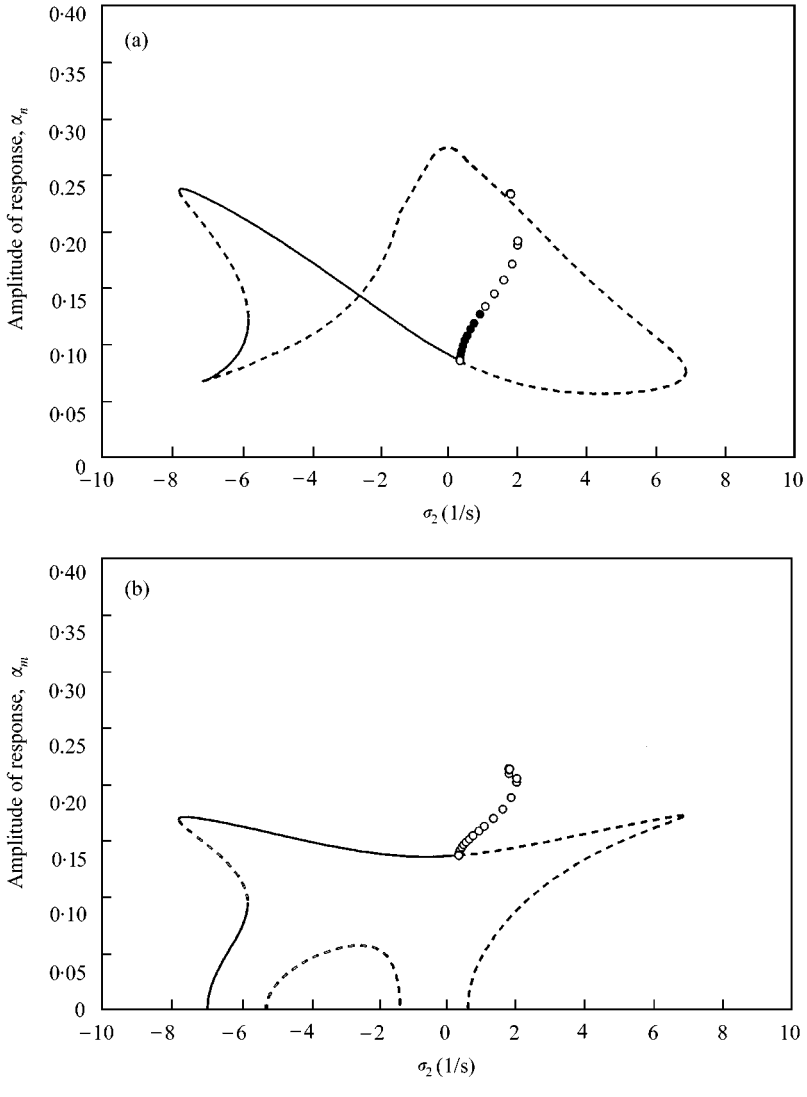

Figure 8. Frequency-response curves obtained by the discretization multiple scales method, $\alpha_m \neq 0$, $\hat{\zeta}_n = 1\%$, $\hat{\zeta}_m = 0{\cdot}3\%$. (a) Amplitude of the rotational mode, (b) amplitude of the transverse mode of span 3: —, stable fixed point; - - - -, unstable fixed points; ●, stable periodic solutions; ○, unstable periodic solutions.

The periodic solutions for modulation amplitude of α_n and α_m, and phases ζ_1 and ζ_2 are shown in Figure 9 for $\sigma_2 = 2{\cdot}844$ Hz at which the amplitudes and phases become periodic. Phase plane curves of modulation amplitude α_n and α_m versus ζ_1 and ζ_2, shown in Figure 10, reflect their limit-cycle behavior.

The frequency of the amplitude modulation of a function of detuning parameter σ_2 is presented in Figure 11. Note that multivalued phenomena exist within certain ranges of σ_2.

The effects of the amplitude of excitation are illustrated in Figure 12. The external detuning parameter σ_2 is chosen as 10 Hz and the internal detuning parameter σ_1 is chosen

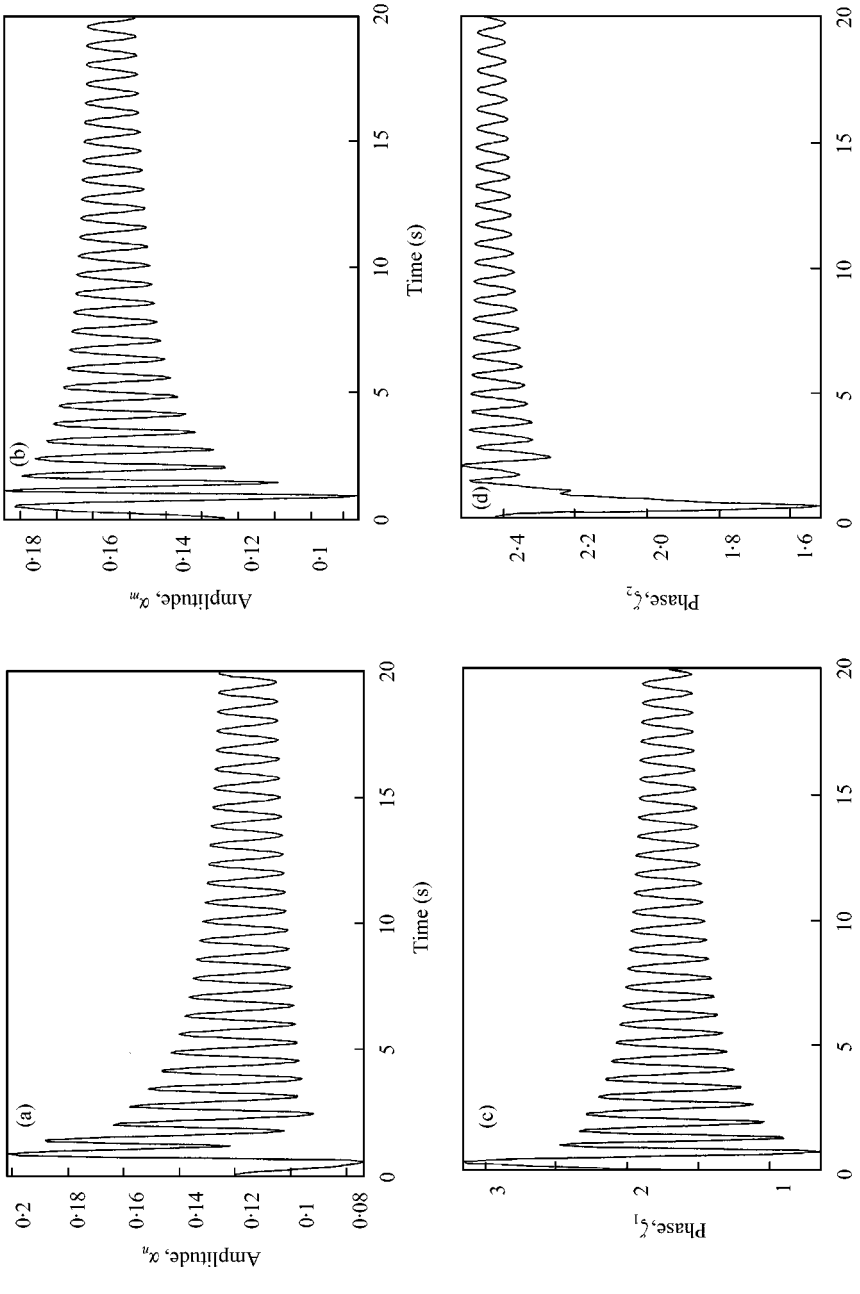

Figure 9. Periodic solutions for $\alpha_n, \alpha_m, \zeta_1$, and ζ_2, $\sigma_2 = 2{\cdot}844$ 1/s. (a) Amplitude of the rotational mode, (b) amplitude of the transverse mode of span 3, (c) phase ζ_1, (d) phase ζ_2.

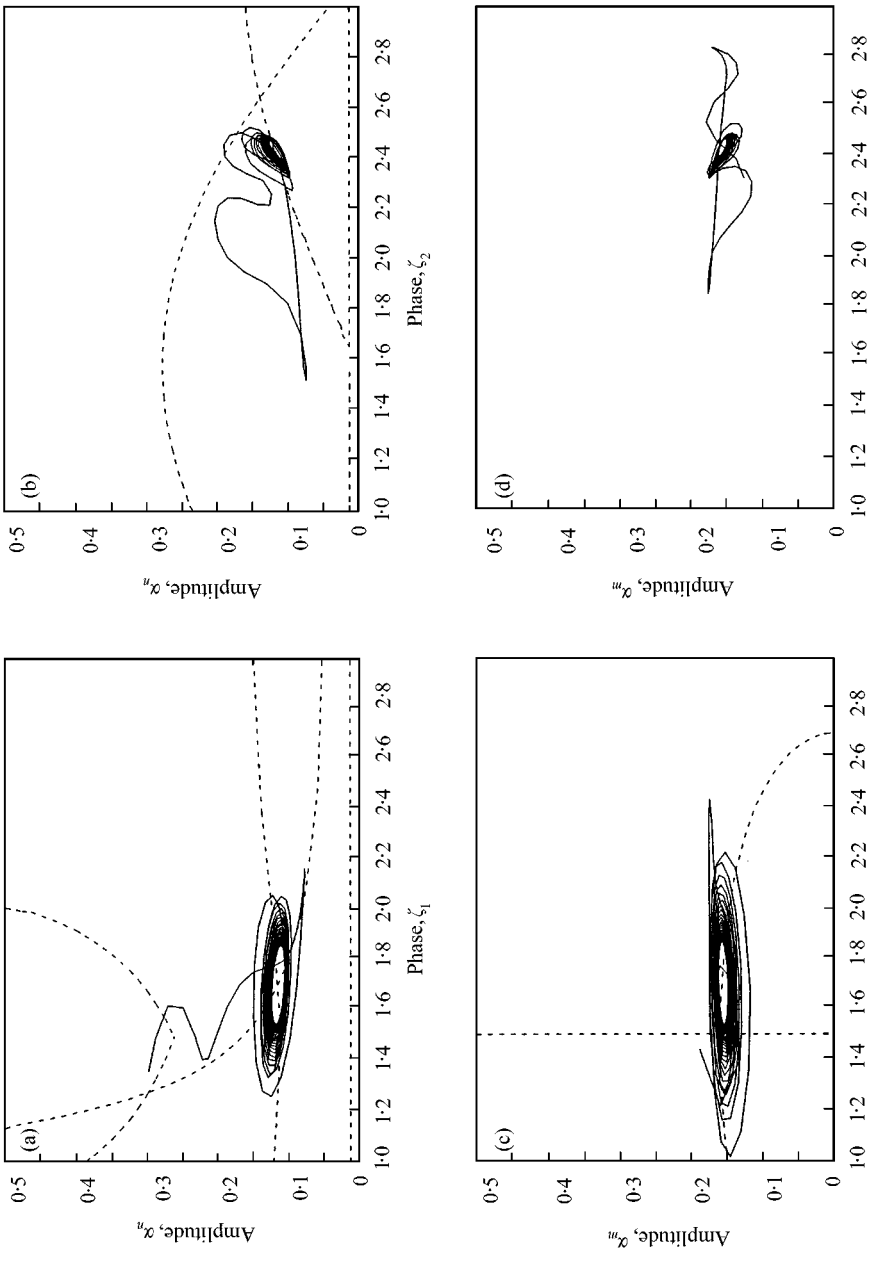

Figure 10. Phase plane curves, $\sigma_2 = 2{\cdot}844$ 1/s. (a) Amplitude of the rotational mode with phase ζ_1, (b) amplitude of the transverse mode of span 3 with phase ζ_1, (c) amplitude of the rotational mode with phase ζ_2, (d) amplitude of the transverse mode of span 3 with phase ζ_2.

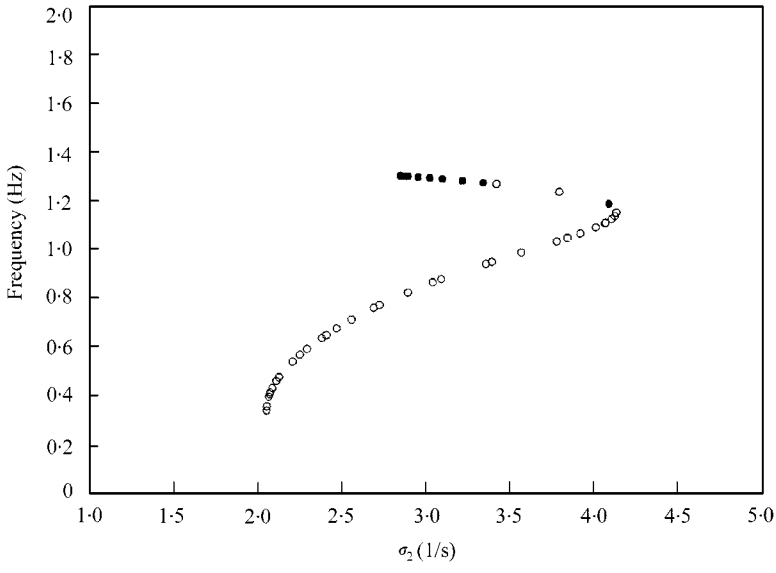

Figure 11. Relation between frequencies of modulated periodic solutions and external detuning parameter σ_2 starting at $\sigma_2 = 2{\cdot}844$; ●, stable periodic solution; ○, unstable periodic solutions.

as 5·95989 Hz. As the excitation level is increased from low levels, the steady state response is zero initially. When the excitation reaches a certain level, the response jumps to attain a high amplitude. Note that the stable area is very small. It happens only at the tip of the curve and is difficult to observe.

Figure 13 shows the effect of the internal detuning parameter σ_1. The external detuning parameter σ_2 is set as 10 Hz and the excitation amplitude is set as 0·5. The results are also different from those obtained from discretization multiple scales method.

The numerical solutions for one-to-one internal resonance show that the discrepancy between the two approaches are quite large. The reason is that the one-to-one internal resonance is due to the cubic non-linearity and the belt drive system involves quadratic and cubic non-linearities. The spatial variation used in the discretization multiple scales method is incomplete since components of the non-linearity in the origianl system that are orthogonal to the linear mode shapes are discarded during the discretization.

6. CONCLUSIONS

In this paper, an analytical approach for the non-linear analysis serpentine belt drive systems is presented. The method of multiple scales is used to treat the continuous governing partial differential equations directly. No assumptions regarding the spatial dependence of the motion are made. It is found that spatial solutions at the second order are different from the linear eigenfunctions of the system. These spatial solutions have a strong influence on the modulation equations governing the first order amplitudes and phase of the motion, which are determined from the third order equations. Therefore, discrepancies exist between the direct multiple scales method and the commonly used multiple scales method in which linear spatial solutions are assumed *a priori* to describe the spatial solutions of the non-linear problem.

The discrepancy for one-to-one internal resonance between the two approaches is particularly large. The quadratic non-linearity dominates for discretization multiple scales

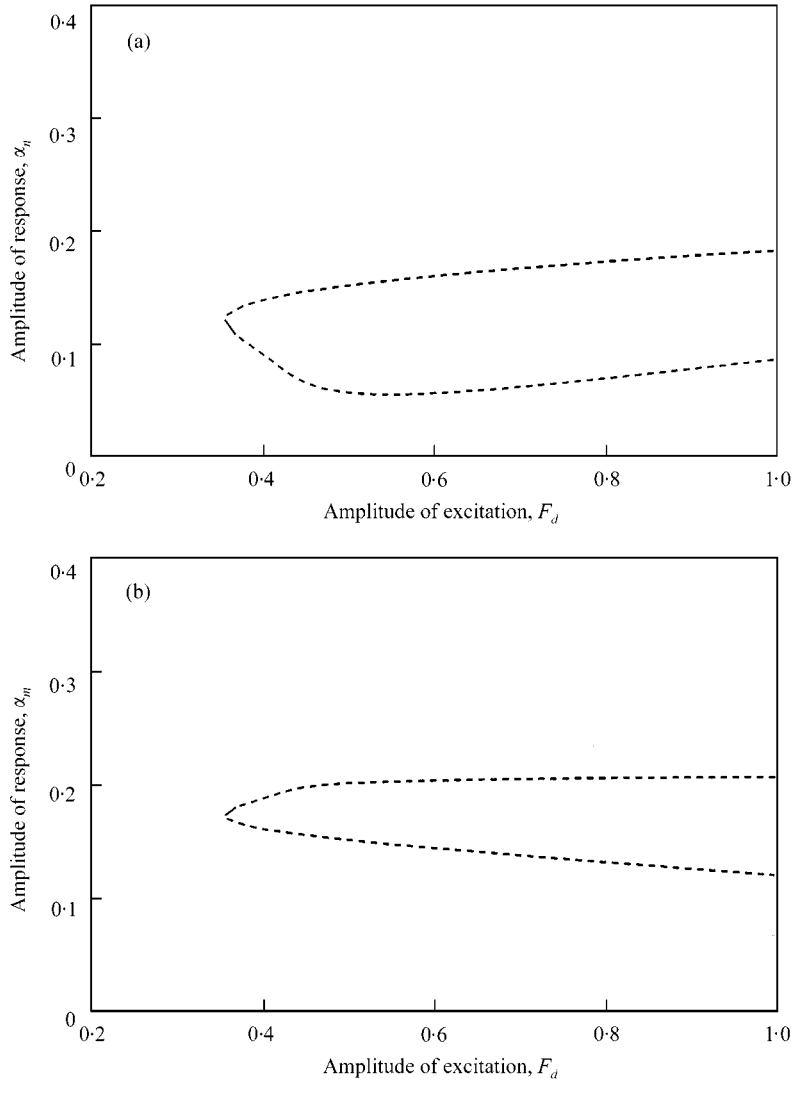

Figure 12. Effect of excitation amplitude, $\sigma_1 = 5{\cdot}95989$ 1/s and $\sigma_2 = 10{\cdot}0$ 1/s. (a) Amplitude of the rotational mode, (b) amplitude of the transverse mode of span 3: —, stable fixed points; - - - , unstable fixed points.

method while the cubic non-linearity dominates for direct multiple scales method in the case of $\alpha_m = 0$. The Hopf bifurcation, the relation between response and excitation amplitude, and the relation between response and excitation frequency for the two approaches are also quite different.

The entire serpentine belt drive system is divided into two subsystems. Transverse motion of subsystem 1 may be parametrically excited through the linear component of the dynamic tension under 1 : 1 resonance conditions while subsystem 2 is also excited by the non-linear components of the dynamic tension which are due to transverse vibration of subsystem 1.

The effect of the internal resonance has been investigated. For large values of detuning parameter σ_1, the system is far from resonance and there is only one solution. When the system is near or at exact one-to-one internal resonance, the response becomes very large

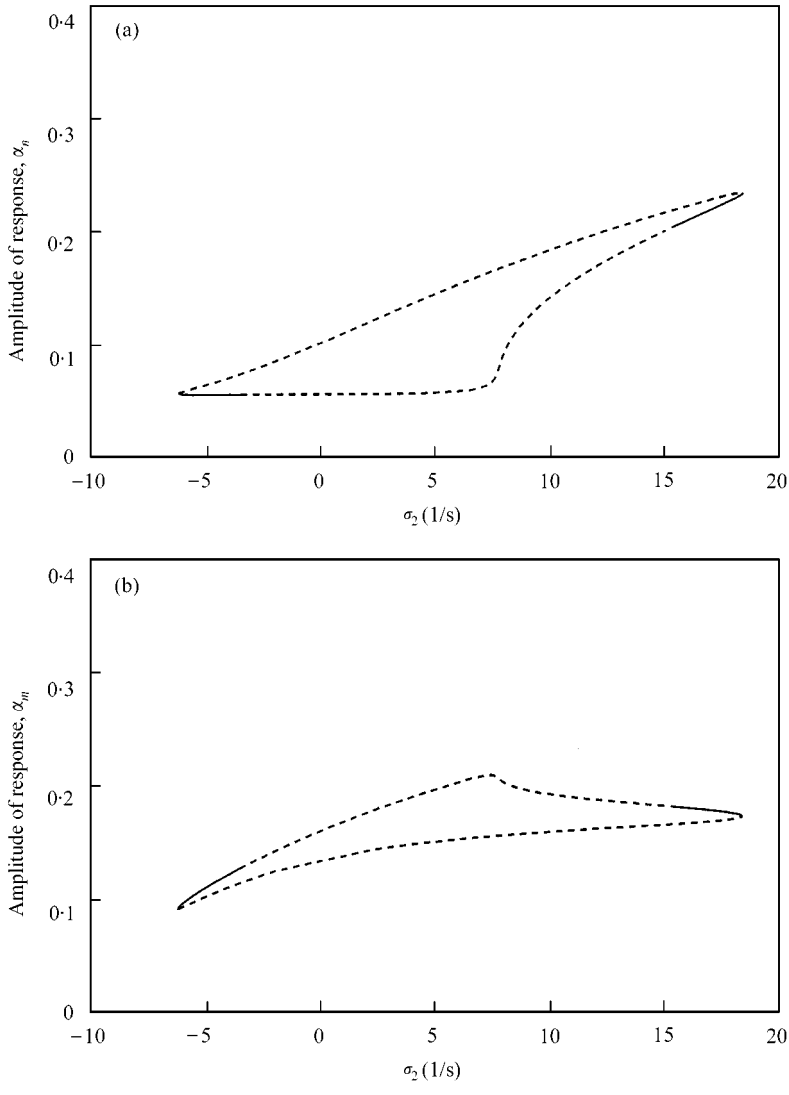

Figure 13. Effect of internal detuning parameter σ_1; $\sigma_2 = 10{\cdot}0$ 1/s and $F_d = 0{\cdot}5$. (a) Amplitude of the rotational mode, (b) amplitude of the transverse mode of span 3: ——, stable fixed points; - - - -, unstable fixed points.

and shows a typical multi-valued non-linear phenomenon. Moving the excitation frequency away from the rotation mode frequency significantly increases the excitation level necessary to produce parametric resonance.

The results presented in this paper indicate the possibility of complicated bifurcations in serpentine belt drive systems. For a certain range of detuning parameter σ_2, the steady state solutions for the amplitudes and phases of serpentine belt drive system undergo Hopf bifurcation. The resulting system response could be amplitude-modulated motion.

ACKNOWLEDGMENT

This research is financially supported by a research grant from Materials and Manufacturing Ontario in Canada.

REFERENCES

1. L. E. HAWKER 1991 *Ph.D. Dissertation, University of Windsor, Ontario, Canada.* A vibration analysis of automotive serpentine accessory drive systems.
2. S. J. HWANG, N. C. PERKINS, A. G. ULSOY and R. J. MECKSTROTH 1994 *ASME Journal of Vibration and Acoustics* **116**, 71–78. Rotational response and slip prediction of serpentine belt drive systems.
3. T. C. KRAVER, G. W. FAN and J. J. SHAH 1996 *ASME Journal of Mechanical Design* **118**, 306–311. Complex modal analysis of a flat belt pulley system with belt damping and coulomb-damped tensioner.
4. C. D. MOTE JR 1996 *ASME Journal of Applied Mechanics* **33**, 463–464. On the non-linear oscillation of an axially moving string.
5. V. A. BAPAT and P. SRINIVASAN 1967 *ASME Journal of Applied Mechanics* **34**, 775–777. Non-linear transverse oscillation in traveling strings by the method of harmonic balance.
6. A. G. ULSOY, J. E. WHITSELL and M. D. HOOVEN 1985 *ASME Journal of Vibrations, Acoustics Stress, and Reliability in Design* **107**, 282–290. Design of belt-tensioner systems for dynamic stability.
7. J. A. WICKERT and C. D. MOTE JR 1990 *ASME Journal of Applied Mechanics* **57**, 738–744, Classical vibration analysis of axially moving continua.
8. J. MOON and J. A. WICKERT 1997 *Journal of Sound and Vibration* **200**, 419–431. Non-linear vibration of power transmission belts.
9. L. ZHANG and J. W. ZU 1998 *Journal of Sound and Vibration* **216**, 75–91. Nonlinear vibrations of viscoelastic moving belts, Part 1: free vibration analysis.
10. L. ZHANG and J. W. ZU 1998 *Journal of Sound and Vibration* **216**, 93–105. Nonlinear vibrations of viscoelastic moving belts, Part 2: forced vibration analysis.
11. R. S. BEIKMANN, N. C. PERKINS and A. G. ULSOY 1996a *ASME Journal of Vibration and Acoustics* **118**, 406–413. Free vibration of serpentine belt drive systems.
12. L. ZHANG and J. W. ZU 1998 *Journal of Sound and Vibration.* Modal analysis of serpentine belt drive systems (accepted).
13. R. S. BEIKMANN, N. C. PERKINS and A. G. ULSOY 1996 *ASME Journal of Vibration and Acoustics* **118**, 567–574. Nonlinear coupled vibration response of serpentine belt drive systems.
14. S. A. PAKDEMIRLI, S. A. NAYFEH and A. H. NAYFEH 1995 *Nonlinear Dynamics* **8**, 65–83. Analysis of one-to-one auto-parametric resonance in cables—discretization vs. direct treatment.

APPENDIX A: EXPRESSIONS OF Γ_{ij}

$$\Gamma_{11} = k_1(\hat{\chi}_{3n}\cos\psi_1 + \hat{\chi}_{2n} - \hat{\chi}_{1n})\left(\frac{\partial^2\gamma_{21}}{\partial x^2} + \frac{\partial^2\gamma_{11}}{\partial x^2}\right) + k_1(\gamma_{15}\cos\psi_1 + \gamma_{14} - \gamma_{13})\frac{\partial^2\bar{\phi}_{1n}}{\partial x^2}$$

$$+ k_1(\gamma_{25}\cos\psi_1 + \gamma_{24} - \gamma_{23})\frac{\partial^2\phi_{1n}}{\partial x^2} + \frac{EA}{2l_1}\left[\int_0^{l_1}\left(\frac{\partial\phi_{1n}}{\partial x}\right)^2 \mathrm{d}x\,\frac{\partial^2\bar{\phi}_{1n}}{\partial x^2} + \int_0^{l_1} 2\,\frac{\partial\phi_{1n}}{\partial x}\frac{\partial\bar{\phi}_{1n}}{\partial x}\mathrm{d}x\,\frac{\partial^2\phi_{1n}}{\partial x^2}\right], \tag{A1}$$

$$\Gamma_{12} = k_2(\hat{\chi}_{3n}\cos\psi_2 + \hat{\chi}_{4n} - \hat{\chi}_{2n})\left(\frac{\partial^2\gamma_{22}}{\partial x^2} + \frac{\partial^2\gamma_{12}}{\partial x^2}\right) + k_2(\gamma_{15}\cos\psi_2 + \gamma_{16} - \gamma_{14})\frac{\partial^2\bar{\phi}_{2n}}{\partial x^2}$$

$$+ k_2(\gamma_{25}\cos\psi_2 + \gamma_{26} - \gamma_{24})\frac{\partial^2\phi_{2n}}{\partial x^2} + \frac{EA}{2l_2}\left[\int_0^{l_2}\left(\frac{\partial\phi_{2n}}{\partial x}\right)^2 \mathrm{d}x\,\frac{\partial^2\bar{\phi}_{2n}}{\partial x^2} + \int_0^{l_2} 2\,\frac{\partial\phi_{2n}}{\partial x}\frac{\partial\bar{\phi}_{2n}}{\partial x}\mathrm{d}x\,\frac{\partial^2\phi_{2n}}{\partial x^2}\right], \tag{A2}$$

$$\Gamma_{13} = \frac{EA}{l_1}\int_0^{l_1}\left(\frac{\partial\phi_{1n}}{\partial x}\frac{\partial\gamma_{21}}{\partial x} + \frac{\partial\bar{\phi}_{1n}}{\partial x}\frac{\partial\gamma_{11}}{\partial x}\right)\mathrm{d}x, \tag{A3}$$

$$\Gamma_{14} = \frac{EA}{l_2}\int_0^{l_2}\left(\frac{\partial\phi_{2n}}{\partial x}\frac{\partial\gamma_{22}}{\partial x} + \frac{\partial\bar{\phi}_{2n}}{\partial x}\frac{\partial\gamma_{12}}{\partial x}\right)\mathrm{d}x - \frac{EA}{l_1}\int_0^{l_1}\left(\frac{\partial\phi_{1n}}{\partial x}\frac{\partial\gamma_{21}}{\partial x} + \frac{\partial\bar{\phi}_{1n}}{\partial x}\frac{\partial\gamma_{11}}{\partial x}\right)\mathrm{d}x, \tag{A4}$$

$$\Gamma_{15} = -\frac{EA}{l_2}\int_0^{l_2}\left(\frac{\partial\phi_{2n}}{\partial x}\frac{\partial\gamma_{22}}{\partial x} + \frac{\partial\bar{\phi}_{2n}}{\partial x}\frac{\partial\gamma_{12}}{\partial x}\right)\mathrm{d}x\cos\psi_2$$

$$-\frac{EA}{l_1}\int_0^{l_1}\left(\frac{\partial\phi_{1n}}{\partial x}\frac{\partial\gamma_{21}}{\partial x} + \frac{\partial\bar{\phi}_{1n}}{\partial x}\frac{\partial\gamma_{11}}{\partial x}\right)\mathrm{d}x\cos\psi_1, \tag{A5}$$

$$\Gamma_{16} = -\frac{EA}{l_2}\int_0^{l_2}\left(\frac{\partial\phi_{2n}}{\partial x}\frac{\partial\gamma_{22}}{\partial x} + \frac{\partial\bar{\phi}_{2n}}{\partial x}\frac{\partial\gamma_{12}}{\partial x}\right)\mathrm{d}x, \tag{A6}$$

$$\Gamma_{21} = k_1(\gamma_{45}\cos\psi_1 + \gamma_{44} - \gamma_{43})\frac{\partial^2\phi_{1n}}{\partial x^2}, \tag{A7}$$

$$\Gamma_{22} = k_2(\gamma_{45}\cos\psi_2 + \gamma_{46} - \gamma_{44})\frac{\partial^2\phi_{2n}}{\partial x^2}, \tag{A8}$$

$$\Gamma_{23} = \frac{EA}{l_1}\int_0^{l_1}\left(\frac{\partial\phi_{1n}}{\partial x}\frac{\partial\gamma_{41}}{\partial x}\right)\mathrm{d}x - \frac{EA}{l_3}\int_0^{l_3}\left(\frac{\partial\phi_m}{\partial x}\frac{\partial\gamma_{61}}{\partial x} + \frac{\partial\bar{\varphi}_m}{\partial x}\frac{\partial\gamma_{51}}{\partial x}\right)\mathrm{d}x, \tag{A9}$$

$$\Gamma_{24} = \frac{EA}{l_2}\int_0^{l_2}\left(\frac{\partial\phi_{2n}}{\partial x}\frac{\partial\gamma_{42}}{\partial x}\right)\mathrm{d}x - \frac{EA}{l_2}\int_0^{l_1}\left(\frac{\partial\phi_{1n}}{\partial x}\frac{\partial\gamma_{41}}{\partial x}\right)\mathrm{d}x, \tag{A10}$$

$$\Gamma_{25} = -\frac{EA}{l_2}\int_0^{l_2}\left(\frac{\partial\phi_{2n}}{\partial x}\frac{\partial\gamma_{42}}{\partial x}\right)\mathrm{d}x\cos\psi_2 - \frac{EA}{l_2}\int_0^{l_1}\left(\frac{\partial\phi_{1n}}{\partial x}\frac{\partial\gamma_{41}}{\partial x}\right)\mathrm{d}x\cos\psi_1, \tag{A11}$$

$$\Gamma_{26} = \frac{EA}{l_3}\int_0^{l_3}\left(\frac{\partial\varphi_m}{\partial x}\frac{\partial\gamma_{61}}{\partial x} + \frac{\partial\bar{\varphi}_m}{\partial x}\frac{\partial\gamma_{51}}{\partial x}\right)\mathrm{d}x - \frac{EA}{l_2}\int_0^{l_2}\left(\frac{\partial\phi_{2n}}{\partial x}\frac{\partial\gamma_{42}}{\partial x}\right)\mathrm{d}x, \tag{A12}$$

$$\Gamma_{31} = k_1(\hat{\chi}_{3n}\cos\psi_1 + \hat{\chi}_{2n} - \hat{\chi}_{1n})\frac{\partial^2\gamma_{31}}{\partial x^2} + k_1(\gamma_{35}\cos\psi_1 + \gamma_{34} - \gamma_{33})\frac{\partial^2\bar{\phi}_{1n}}{\partial x^2}, \tag{A13}$$

$$\Gamma_{32} = k_2(\hat{\chi}_{3n}\cos\psi_2 + \hat{\chi}_{4n} - \hat{\chi}_{1n})\frac{\partial^2\gamma_{32}}{\partial x^2} + k_2(\gamma_{35}\cos\psi_2 + \gamma_{36} - \gamma_{34})\frac{\partial^2\bar{\phi}_{2n}}{\partial x^2}, \tag{A14}$$

$$\Gamma_{33} = \frac{EA}{l_1}\int_0^{l_1}\left(\frac{\partial\bar{\phi}_{1n}}{\partial x}\frac{\partial\gamma_{31}}{\partial x}\right)\mathrm{d}x - \frac{EA}{l_3}\int_0^{l_3}\left(\frac{\partial\varphi_m}{\partial x}\frac{\partial\bar{\gamma}_{61}}{\partial x}\right)\mathrm{d}x, \tag{A15}$$

$$\Gamma_{34} = \frac{EA}{l_2}\int_0^{l_2}\left(\frac{\partial\bar{\phi}_{2n}}{\partial x}\frac{\partial\gamma_{32}}{\partial x}\right)\mathrm{d}x - \frac{EA}{l_1}\int_0^{l_1}\left(\frac{\partial\bar{\phi}_{1n}}{\partial x}\frac{\partial\gamma_{31}}{\partial x}\right)\mathrm{d}x, \tag{A16}$$

$$\Gamma_{35} = -\frac{EA}{l_2}\int_0^{l_2}\left(\frac{\partial\bar{\phi}_{2n}}{\partial x}\frac{\partial\gamma_{32}}{\partial x}\right)\mathrm{d}x\cos\psi_2 - \frac{EA}{l_1}\int_0^{l_1}\left(\frac{\partial\bar{\phi}_{1n}}{\partial x}\frac{\partial\gamma_{31}}{\partial x}\right)\mathrm{d}x\cos\psi_1, \tag{A17}$$

$$\Gamma_{36} = \frac{EA}{l_3}\int_0^{l_3}\left(\frac{\partial\varphi_m}{\partial x}\frac{\partial\bar{\gamma}_{61}}{\partial x}\right)\mathrm{d}x - \frac{EA}{l_2}\int_0^{l_2}\left(\frac{\partial\bar{\phi}_{2n}}{\partial x}\frac{\partial\gamma_{32}}{\partial x}\right)\mathrm{d}x, \tag{A18}$$

$$\Gamma_{41} = k_3(\hat{\chi}_{1n} - \hat{\chi}_{4n})\gamma_{61} + k_3(\gamma_{13} - \gamma_{16})\frac{\partial^2\bar{\varphi}_m}{\partial x^2}, \tag{A19}$$

$$\Gamma_{51} = k_3(\hat{\chi}_{1n} - \hat{\chi}_{4n})\gamma_{61} + k_3(\hat{\chi}_{1n} - \hat{\chi}_{4n})\gamma_{51} + k_3(\gamma_{23} - \gamma_{26})\frac{\partial^2\varphi_m}{\partial x^2}, \tag{A20}$$

$$\Gamma_{61} = k_3(\gamma_{33} - \gamma_{36})\frac{\partial^2\bar{\varphi}_m}{\partial x^2} + k_3(\gamma_{43} - \gamma_{46})\frac{\partial^2\varphi_m}{\partial x^2}. \tag{A21}$$